32ND INTERNATIONAL COSMIC RAY CONFERENCE, BEIJING 2011

A multi-wavelength view of the large γ-ray flares from Mrk421 in 2010

H.H. HE[1], S.Z. CHEN[1], L. ZHANG [2] ON BEHALF OF THE ARGO-YBJ COLLABORATION
[1]*Particle & Astrophysics Center, Institute of High Energy Physics, CAS, Beijing, China.*
[2]*Department of Physics, Yunnan University, Kunming, China*
chensz@ihep.ac.cn

Abstract: As the most active blazar, Mrk421 is an excellent candidate for the study of the physical processes within the jets of AGN. Since 2008 August, this source has been simultaneously monitored by the ARGO-YBJ experiment at γ-ray energies above 0.3 TeV, LAT/Fermi at γ-ray energies 0.1-300GeV, BAT/$Swift$ at hard X-ray 15-50 keV and ASM/$RXTE$ at soft X-ray 2-12 keV day by day. Here, we report a multi-wavelength view of the large flare from Mrk421 in 2010 February, which is the first large flare simultaneously observed by the four detectors. 2 months later, a likely "orphan" γ-ray flare is observed. To study the mechanism of the flares, modeling with the synchrotron self-Compton process is constructed. For comparison, the simultaneous multi-wavelength spectra averaged during a long-term from 2008 August to 2011 February are also presented, where a connection between Fermi and ARGO-YBJ is achieved at energy around 300 GeV.

Keywords: Mrk 421, gamma ray observation, AGN, ARGO-YBJ

1 Introduction

Mrk 421 (z=0.031) is one of the brightest blazars known and is classified as a BL Lac object, a subclass of active galactic nuclei (AGNs). Its emission, like that of the other blazars, is dominated by non-thermal radiation from a relativistic jet which is aligned along our line of sight. The spectral energy distribution (SED) is double-humped at X-ray and γ-ray energies in a plot of νF_ν versus ν [1], where ν is the frequency and F_ν is the flux density. The lower component is usually interpreted to be caused by the synchrotron radiation from relativistic electrons (and positrons) within the jet. The origin of The higher component is under debate. Many models attribute the high energy emission to the inverse Compton scattering of the synchrotron (synchrotron self-Compton, SSC) or external photons (external Compton, EC) by the same population of relativistic electrons [2, 3], therefore a X-ray/γ-ray correlation would be expected. Other models invoke hadronic processes including proton-initiated cascades and/or proton-synchrotron emission in a magnetic field-dominated jet [4].

Mrk 421 is a very active blazar with major outbursts about once every two years in both X-ray and γ-ray. A major outburst usually lasts several months and is accompanied by many rapid flares with timescales from tens of minutes to several days. Its high variability and broadband emission require long-term, well-sampled, multi-wavelength observations in order to understand the emission mechanisms of these outbursts. During the last decade, several coordinated multi-wavelength campaigns focusing on Mrk 421 have been conducted both in response to strong outbursts and as part of dedicated observing campaigns (for a review see [5]). Some important general features of the AGN flares are obtained. Although X-rays and γ-rays are found strongly correlated, they are not evidently correlated with optical and radio emissions. The spectral index becomes harder at higher fluxes in both X-ray and γ-ray bands. All these phenomena can be interpreted in the framework of the SSC model. However, "orphan flares", which have only γ-ray emission without low energy companions, or a lag of about 2 days between X-rays and γ-rays [6] are usually recognized as major challenges to the model. Recently, a long-term continuous monitoring of Mrk421 has been performed between the ARGO-YBJ experiment and satellite-borne X-ray detector [7], which gives a systematic analysis between very high energy (VHE) γ-rays and X-ray. Both the temporal and spectral results strongly support the predictions of the SSC model.

The ARGO-YBJ experiment [8] is a wide field-of-view (FOV) air shower experiment. It is operated day and night with a duty cycle higher than 86% and can observe any source with a zenith angle less than 50°. It has been continuously monitoring the northern sky for outbursts from all AGNs such as Mrk 421 since 2006 July. Meanwhile, these sources are also monitored by the satellite-borne X-ray detectors ASM/$RXTE$ and BAT/$Swift$. In 2008 August, Fermi began to monitor the whole sky at energy above 100 MeV, which connects with the observation of the ARGO-YBJ experiment around 300 GeV. Combining these detectors, continuous simultaneous multi-wavelength observa-

tions can be naturally achieved without coordinated campaigns, which is essential in investigating the temporal features of AGN emissions. In 2010 February, a strong flare at VHE γ-ray and X-ray from Mrk 421 was alarmed by the VERITAS collaboration [9] and the MAXI team [10]. This flare was clearly seen also by ARGO-YBJ, ASM/$RXTE$ and BAT/$Swift$ during the long-term monitoring analysis [7]. Especially, this is the first large γ-ray observed simultaneously by ARGO-YBJ and Fermi. In this paper, we report on the multi-wavelength view of the large γ-ray flares from Mrk421 in 2010.

2 Observations and data analysis

2.1 VHE γ-ray data

The ARGO-YBJ experiment [8] is an extensive air shower array with full coverage RPC detectors at Yangbajing (4300 m a.s.l., Tibet, China). It is the result of a collaboration among Chinese and Italian institutions and is designed for VHE γ-ray astronomy and cosmic ray observations. The central 130 clusters began taking data in 2006 July, and the "guard ring" was merged into the DAQ stream in 2007 November. The trigger rate is $\sim$3.5 kHz with a dead time of 4% and the average duty cycle is higher than 86%. To achieve a better angular resolution, the event selections used in [7] is applied here and only events with a zenith angle less than 50° are used. In order to extract an excess of γ-rays from the source, the so-called "direct integral method" [12] is applied to estimate the number of cosmic ray background events. To remove the affection of cosmic ray anisotropy, a correction has been applied which can be found in [7]. The Li-Ma formula [13] is used to estimate the significance.

2.2 HE γ-ray data

LAT/$Fermi$ is a pair-conversion telescope, with a FOV over 2 sr, active in the 30 MeV$-$400 GeV energy range with an unprecedented sensitivity. $Fermi$ has begun to monitor the whole sky on a daily basis since 2008 August. In this work, we use the LAT data from a region of 10° radius centered on Mrk 421. The analysis is performed using the ScienceTools, provided by the $Fermi$ collaboration (Version v9r18p6) [14]. Events with zenith angles $< 105^\circ$ are selected from the "diffuse" class, which have the highest probability of being photons. The light curve is created through aperture photometry, which is model independent while without subtracting the background. To estimate the source SED, we used the gtlike tool, which exploits a maximum likelihood method. The instrument response function is $P6\_V3\_DIFFUSE$ and the Galactic emission is reproduced using the model $gll\_iem\_v02.fit2$. All sources listed in the LAT/$Fermi$ first year Catalogue within 10° from the Mrk 421 position are taken into account in the likelihood analysis.

2.3 Hard X-ray data

The BAT/$Swift$ is a highly sensitive, large FOV instrument designed to provide critical GRB triggers. It is a coded aperture imaging instrument with a FOV 1.4 sr. With rather a long exposure by orbiting the Earth every 1.5 hours, the data from the BAT/$Swift$ can also produce a sensitive hard X-ray all-sky survey. The data publicly provided by BAT/$Swift$ [1] are used in this work. For Mrk 421 the provided daily flux at energy 15-50 keV started from 2005 February.

2.4 Soft X-ray data

The ASM/$RXTE$ consists of three proportional counters, each of which has a $6^\circ \times 90^\circ$ FOV, and covers about 80% of the sky upon the completion of one full rotation, which takes about 1.5 hr. The ASM data (2$-$12 keV) are publicly available [2]. We obtained the light curves of Mrk 421 from the MIT archive. The light curves come in three energy bands: 1.5$-$3, 3$-$5, and 5$-$12 keV, which are used to estimate the X-ray spectrum in this work.

3 Results

3.1 Light curves

Figure 1 show the light curves of Mrk 421 in four energy bands from Soft X-ray to VHE γ-ray. The ARGO-YBJ curve is obtained using events with $N_{pad} > 100$, thus the median energy of the observed photons is 1.8 TeV, assuming a spectral index -2.4. The soft X-ray (2$-$12 keV) flux increased to a flux 95.9($\pm$4.6) and 94.1($\pm$4.3) mCrab on 2010 February 16 and 17, respectively, from 21.0($\pm$3.9) mCrab on February 14. Afterward, a high flux around 50 mCrab lasted two weeks. A similar variation also appears in the light curve of hard X-ray (15$-$50 keV), with a peak flux 24.2($\pm$3.7) mCrab on February 16. A γ-ray flare consistent with the X-ray flare on February 16 is visible in the light curves of HE and VHE γ-ray. To reduce the affection of fluctuation, a smoothing technique has been applied to the light curves of γ-ray, which means each point in panels (c) and (d) is the event rate averaged over five days centered on it. This flare is associated with the strong VHE γ-ray activity detected by the VERITAS Observatory on February 17[9]. Unlike the long-lived flaring in X-ray, the flux in HE γ-ray decreases to a normal level shortly after the peak flux, while the flare in VHE γ-ray seems to last as long as that in X-ray. It can be concluded that the strong flare on February 16 is detected in all four energy bands from soft X-ray to VHE γ-ray and their time of peak flux are consistent with each other.

1. Transient monitor results provided by the BAT/$Swift$ team: http://heasarc.gsfc.nasa.gov/docs/swift/results/transients/weak/Mrk421/.

2. Quick-look results provided by the ASM/$RXTE$ team: http://xte.mit.edu/ASM_lc.html.

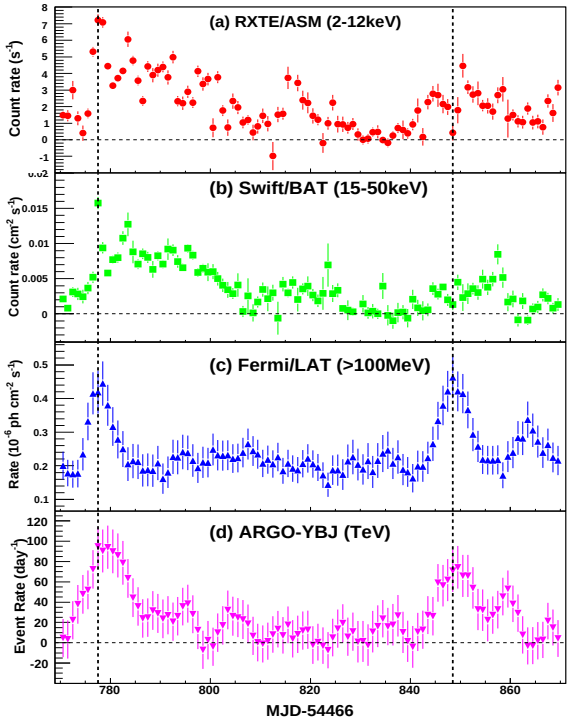

Figure 1: Daily light curve of Mrk 421. The panels (a) and (b) show the daily count rate in the $2-12$ keV and $15-50$ keV measured by ASM/$RXTE$ and BAT/$Swift$, respectively. The panels (c) and (d) show the daily event rate in >100MeV and TeV bands measured by LAT/$Fermi$ and ARGO-YBJ, respectively, both of which have been smoothed and each point is the event rate averaged over five days. The two vertical dashed lines indicate the time of peak flux of the two flares on 2010 February 16 and 2010 April 28. All the errors represent the 1 σ statistical one.

Besides the one on February 16, another flare with peak time on 2010 April 28 is visible in light curves of HE and VHE γ-ray, while no counterparts in soft and hard X-ray are observed, therefore, it may be an "orphan" γ-ray flare. Unlike previous reported "orphan" flares [6], the observation is continuous. Especially, at both X-ray and γ-ray bands, there are two independent measurements to cross check. Even if no significant large flare is in the light curves of X-ray, flux is not stable during this period. The so-called "orphan" γ-ray flare may be correlated with the X-ray band.

3.2 Spectral Energy Distribution

According to Figure 1, we choose the period of the first flare (denoted as flare 1) from 2010 February 14 to 23. For the second flare (denoted as flare 2), the period is chosen from 2010 April 25 to May 2. The time averaged SEDs from X-ray to VHE γ-ray are summarized in Table 1, where a simple power law is assumed, F is the integral flux and α is the spectral index. For comparison, simultaneous

Table 1: SED results, the unit for flux is (ph cm^{-2} s^{-1})

Energy	flare 1	flare 2	long-term
F(2-12keV)	0.201	0.096	0.056
α	-1.94±0.04	-1.83±0.18	-2.20±0.03
F(0.1-400GeV)	2.3×10^{-7}	3.9×10^{-7}	1.9×10^{-7}
α	-1.67±0.08	-1.85±0.02	-1.83±0.01
F(0.5-10TeV)	36.4×10^{-11}	36.9×10^{-11}	7.5×10^{-11}
α	-2.11±0.25	-2.32±0.36	-2.54±0.13

averaged SEDs over a long-term period, from 2008 August 5 to 2011 February 8 including the two flares, are also presented in Table 1. To remove the influence caused by absorption of γ-rays in the extragalactic background light, we adopt the optical depth estimated by Franceschini [16]. During the flare 1, the SEDs become harder at all three energy bands comparing the long-term averaged SEDs. The flux in X-ray and VHE bands increases about 4 and 5 times, respectively. A similar evolution are also presented during flare 2, while the spectrum in X-ray is harder than flare 1 even if the flux is only 1.7 times comparing with the long-term flux. The flare 2 in γ-ray, therefore, is correlated with X-ray bands.

3.3 Modelling of the X-ray and γ-ray emissions

A fit to the three flux-averaged SEDs with a homogeneous one-zone SSC model proposed by [15] is performed (see also [17]). In this model, the parameters include the Doppler factor $\delta = 1/[\Gamma(1-\beta\cos\theta)]$, the spherical blob radius R, magnetic field strength B, electron spectral index s, electron maximum Lorentz factor $\gamma_{\rm max}$, and electron injection compactness $l_e = \frac{1}{3}m_e c\sigma_{\rm T}R^2\int_1^\infty d\gamma(\gamma-1)Q_e$, where Γ and $c\beta$ are the Lorentz factor and the speed of the blob, respectively, γ is the electron Lorentz factor, $\sigma_{\rm T}$ is the Thomson cross-section, θ is the angle between its direction of motion and the line of sight of the observer, and Q_e, the electron spectrum at injection, is assumed to follow a power-law $Q_e = q_e\gamma^{-s}\exp(-\gamma/\gamma_{\rm max})$. The best fits are shown in Figure 2 and 3 for flare 1 and flare 2, respectively. For comparison, the best fit for long-term result is also shown, where the points at $14-195$ keV are the 58-month averaged spectrum measured by BAT/$Swift$ [3]. The corresponding parameters for different periods are given in Table 2. Without changing the magnetic field and blob size, the flare 1 and flare 2 can be interpreted as the variation of the injected electron flux and SED. The flare 1 may be mainly caused by the hardening of injected electron SED with increasing the electron maximum energy. The flare 2 may be mainly brought about by the increases of the maximum energy.

3. http://heasarc.gsfc.nasa.gov/docs/swift/results/bs58mon/SWIFT_J1104.4p3812

Table 2: List of the best parameters in SSC model.

Parameters	flare 1	flare 2	long-term
γ_{max}	3×10^6	2×10^6	9×10^5
l_e	1.4×10^{-5}	5×10^{-5}	5×10^{-5}
B (G)	0.15	0.15	0.15
R (cm)	5×10^{16}	5×10^{16}	5×10^{16}
δ	15	15	17
α	1.7	1.8	1.85

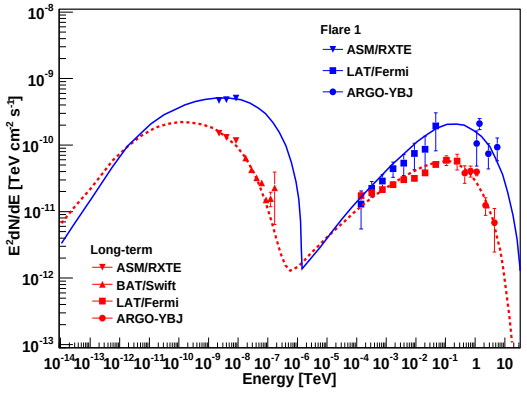

Figure 2: Spectral energy distribution of Mrk 421 derived during the period of flare 1 (blue points) and long-term (red points). The solid and dotted curve shows the best fit to the flare 1 and long-term data, respectively, with an homogeneous one-zone SSC model.

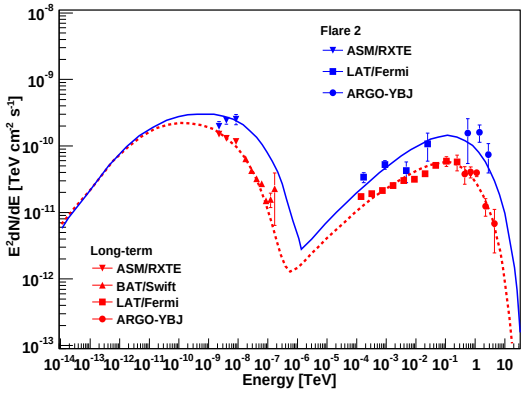

Figure 3: Spectral energy distribution of Mrk 421 derived during the period of flare 2 (blue points) and long-term (red points). The solid and dotted curve shows the best fit to the flare 2 and long-term data, respectively, with an homogeneous one-zone SSC model.

4 Discussion and Conclusion

Mrk 421 is a very active blazar with frequent outbursts, which are composed of many flares. This makes this blazar an excellent candidate for the study of the jet physics in AGNs. In this paper, we have presented a multi-wavelength view of the large γ-ray flares from Mrk421 in 2010. For comparison, a 2.5-year simultaneous multi-wavelength averaged SED are investigated. This SED includes a complete measurement from 100 MeV to 10 TeV. It strictly limits space of the parameters of the models. A strong flare from X-ray, through γ-ray is clearly detected together with spectral hardening, which indicates that the peak energy increases at both X-ray and γ-ray bands. According to our fitting using SSC model, this flare may be caused by the variation of the electron injection spectrum including maximum energy and spectral index. Besides the strong flare, one "orphan" γ-ray flare is observed both by LAT/$Fermi$ and ARGO-YBJ. Even without large flux variation in X-ray, the spectrum becomes much harder, which may be correlated with flare at γ-ray bands. In the framework of SSC model, this so-called "orphan" γ-ray can be plausibly interpreted as the variation of the maximum energy of the electron injection spectrum.

5 acknowledgments

This work is supported in China by NSFC (No.10120130794), the Chinese Ministry of Science and Technology, the Chinese Academy of Sciences, the Key Laboratory of Particle Astrophysics, CAS, and in Italy by the Istituto Nazionale di Fisica Nucleare (INFN). We also acknowledge the essential supports of W.Y. Chen, G. Yang, X.F. Yuan, C.Y. Zhao, R. Assiro, B. Biondo, S. Bricola, F. Budano, A. Corvaglia, B. D'Aquino, R. Esposito, A. Innocente, A. Mangano, E. Pastori, C. Pinto, E. Reali, F. Taurino and A. Zerbini, in the installation, debugging and maintenance of the detector.

References

[1] Fossati, G., et al. 1998, MNRAS, 299, 433
[2] Ghisellini, G., Celotti, A., Fossati, G., et al. 1998, MNRAS, 301, 451
[3] Dermer, C. D., et al. 1992, A&A, 256, L27
[4] Aharonian, F. A., 2000, New Astron., 5, 377
[5] Wagner, R., 2008, arXiv:0808.2483v1.
[6] Blazejowski, M., et al. 2005, ApJ, 630, 130
[7] Bartoli. B., et al. 2011, ApJ, 734,110
[8] Aielli, G., et al. 2006, Nucl. Instrum. Meth. A, 562, 92
[9] Ong, R.A., 2010, ATel#2443
[10] Isobe, N., et al. 2010, Publications of the Astronomical Society of Japan, 62, L55
[11] Aielli, G., et al. 2009c, Nucl. Instrum. Meth. A, 608, 246
[12] Fleysher, R., et al. 2004, ApJ, 603, 355
[13] Li, T.P.,& Ma, Y.Q. 1983, ApJ, 272, 317
[14] Abdo, A.A., et al. 2010, ApJ, 708, 1310
[15] Mastichiadis, A. & Kirk, J.G. 1995, ApJ, 295, 613
[16] Franceschini, A., et al. 2008, A&A, 487, 837
[17] Yang, C.Y., Fang, J., Lin, G.F. & Zhang, L. 2008, ApJ, 682, 767